Study of Selective Laser Melting Process Parameters to Improve the Obtainable Roughness of AlSi10Mg Parts

Luana Bottini

Abstract Selective Laser Melting of AlSi10Mg parts has a lot of applications in different fields such as aerospace and automotive for its abilities to fabricate components characterized by complex shapes, good mechanical properties and low porosity. One of the main drawbacks for its application is the obtainable surface roughness widely not suitable for functional requirements. Typically, the improvement is handled by secondary operations thus markedly increasing the production time and costs. In this paper the possibility to improve the surface roughness by tuning Selective Laser Melting process parameters is investigated. A design of experiments is carried out considering not only the common laser process parameters but also the changing of the contour, upskin and downskin strategy definitions. This way the attained results show a marked decreasing of the roughness for vertical and horizontal surfaces.

Keywords Selective laser melting · AlSi10Mg · Roughness

Nomenclature

SLM	Selective Laser Melting
AM	Additive Manufacturing
b_o	Beam offset
h_o	Contour offset
s_o	Overlapping between lines
h_d	Hatch distance
P	Laser power

L. Bottini (✉)
Departement of Mechanical and Aerospace Engineering, Sapienza University of Rome, via Eudossiana 18, 00184 Rome, Italy
e-mail: luana.bottini@uniroma1.it

© The Editor(s) (if applicable) and The Author(s), under exclusive license to Springer Nature Switzerland AG 2021

E. Ceretti and T. Tolio (eds.), *Selected Topics in Manufacturing*,
Lecture Notes in Mechanical Engineering,
https://doi.org/10.1007/978-3-030-57729-2_9

L	Layer thickness
v	Scan speed
VED	Volumetric Energy Density
LED	Linear Energy Density
R_a	Average roughness
R_t	Peak to valley roughness
R_{sk}	Skewness of profile height
R_{ku}	Kurtosis of profile height
Δ_q	Root mean square of the profile slopes
λ_c	Cut-off
λ_s	Wavelength cut-off

1 Introduction

Selective Laser Melting (SLM) is an Additive Manufacturing (AM) technology that belongs to the category of the power bed fusion [1]: it uses thermal energy provided by a laser source to selectively melts regions of a powder bed. This way it is possible to fabricate layer by layer full dense metallic components characterized by very complex geometries and mechanical properties comparable to those of bulk materials produced by traditional technologies [2]. One of the most used material is the aluminum that has the potential for applications and developments in different fields such as aviation, aerospace, automotive, naval and power electronics due to its low density, high specific strength and good corrosion resistance as well as its excellent electric and thermal conductivity [3–5].

Notwithstanding its industrial diffusion, many issues exist in the SLM processing of aluminum alloys due to their physical properties. The spreading of the powders in thin layers is difficult due to their low density and poor flowability leading to the formation of holes in the powder bed especially in presence of humidity [6]. The low absorptivity at laser wavelength and the high reflectivity require high specific energy [7]. The high thermal conductivity causes a fast cooling and a heat dissipation away from the melt pool [8]. The stirring and the incorporation of the powder oxide film into the melt pool can cause defects inside the part. The oxidized surfaces reduce the wettability of the built part and a high power is necessary to disrupt this oxide allowing the bind of the next layers and the realization of dense components [6].

The quality of SLMed parts depends upon the selection of the process parameters such as the laser power, the scanning speed, the hatch spacing, the layer thickness and the built orientation. The use of improper process parameters can cause defects such as cracks, low density, balling, satellite and dropping [9]. These surface defects deeply affect the roughness that typically is too high to meet the demand of the industrial production. In [10] the authors studied the influence on the surface roughness of the building orientation by the development of a roughness prediction model as a function of the local stratification angle. It highlighted the deep difference of morphology

for surfaces characterized by different building orientations. In [11] the effects of the surface slope with different angles were studied by simulation and experimentation: as the slope increased, the part quality improved but the dimensional deviation worsened.

Calignano et al. [12] used a Taguchi method to study the effect of the laser power, the scan speed and the hatching spacing on surface roughness of horizontal surfaces of AlSi10Mg SLMed parts. They found that the scanning speed has the greatest influence on the surface quality. In [13] the influence of the same process parameters was altered such that better surface roughness for horizontal surfaces could be achieved for AlSi10Mg parts. The results showed that the best outcome was obtained for high specific energy at the lowest experimented beam offset. With this process parameters set also the minimum porosity inside the specimen was reached. In [14] only vertical surfaces were considered: the effect of the laser power, the scanning speed and the linear energy density on the morphologies of single tracks and on the roughness of vertical surfaces of cubic specimens were studied. They found a reduction more than the 70% of the average roughness for energy density in the range of 4.5–7.4 J/cm.

Another chance to reduce the roughness and satisfy functional requirements is the post processing such as surface treatments and machining. Common operations are sand blasting, machining, chemical etching, and plasma spraying but they are skill operator-dependent, labor-intensive, and difficult to apply to complex shape parts [15]. Although the post processing operations improve the surface quality, an increasing of production time and costs is required thus weakening most of the advantages of the SLM process in term of flexibility, efficiency and direct fabrication [10].

A compromise is the use of laser remelting: multiple scanning strategies can be performed during the SLM process on the external surfaces or on the entire layer. In [16] the influence of laser remelting on density, surface quality and staircase effect of AISI 316L SLMed parts was studied varying the operating parameters such as scan speed, laser power and hatch spacing. Moreover, a comparison between the remelting during and after the SLM process for inclined surfaces was done using the same machine. The results showed that when the laser remelting was applied only to the contour during the SLM process the staircase effect was reduced by 10–15%; conversely the remelting after the SLM fabrication provided a reduction of 70% in the average roughness. Notwithstanding the better result of the second strategy, it requires longer time to plan the remelting operation and it is limited to simple convex and accessible shapes. In [17] the remelting of the entire layers of AlSi10Mg part was performed in order to study the variation of the surface roughness of horizontal surfaces, the microstructure, the microhardness, the characteristic of the melt pool and the relative density. The results showed that the laser remelting enhanced the surface roughness and the relative density; it permitted to obtain a shallower melt pool, finer microstructure and higher hardness but it implied longer building time. In [18] a method for the correction of the porosity by remelting was studied: three different scan strategies were considered and experimented. Also, the surface roughness, the geometrical accuracy and material microhardness were evaluated. The results showed that the polishing strategy was the best solution to

improve the porosity and to obtain smooth surfaces free of pits and protruded zones. Vaithilingam et al. [19] investigated the effect on surface chemistry of a double scanning only on the skin of Ti6Al4V components fabricated through SLM: they found that it altered the chemical composition leading to a significant reduction of the corrosion resistant and the biocompatibility but it permitted an improving of the surface quality. This method was effective on horizontal surfaces while inclined ones were not subjected to a significant improvement.

Aim of this work is to improve the obtainable surface roughness of AlSi10Mg parts characterized by surfaces with different inclinations performing a finishing operation directly inside the SLM process. For the purpose a remelting was performed for each layer contour after its fabrication with standard process parameters: the remelting strategy regarded only the external skin, this way the building time is slightly affected by the remelting. Vertical, horizontal and inclined surfaces required different scan strategies thus different remelting approaches were designed. An experimental plane was performed in order to find suitable process parameters for the different scan strategies.

2 Material and Methods

2.1 Machine and Material

The employed machine is an EOSINT®M290 located in the AM Lab of Sapienza University of Rome. It is equipped with a building platform of $250 \times 250 \times 325$ mm^3 and a 400 W Ytterbium fiber continuum laser characterized by a beam spot size of 100 μm. Samples were fabricated using AlSi10Mg gas atomized powder supplied by EOS. It presents the nominal chemical composition reported in Table 1.

2.2 Scan Strategy and Process Parameters Definitions

During the SLM process, the laser beam moves over the surface of the powder bed in order to consolidate a layer. The scanning strategy is typically divided into two types: the part hatching and the part contour. The former is the processing of the internal area of the layer providing part mechanical resistance. The latter is developed according to the layer boundary and allows for better surface quality. A specific laser path must be generated considering geometrical elements and offsets. In Fig. 1 a schematization of the laser path definition is reported.

During the laser scan, namely the exposure, a consolidation zone of the solidified metal forms around the laser beam. The size of this zone depends upon the material used and the exposure parameters set. A beam offset b_o is introduced to compensate for the consolidation zone. The contour part is moved by this value with respect to

Table 1 Chemical composition of the AlSi10Mg powders

Element	Si	Fe	Cu	Mn	Mg	Ni	Zn	Pb	Sn	Ti	Al
Weight (%)	9.0 ÷ 11	≤0.55	≤0.05	≤0.45	0.2 ÷ 0.45	≤0.05	≤0.10	≤0.05	≤0.05	≤0.15	Balance

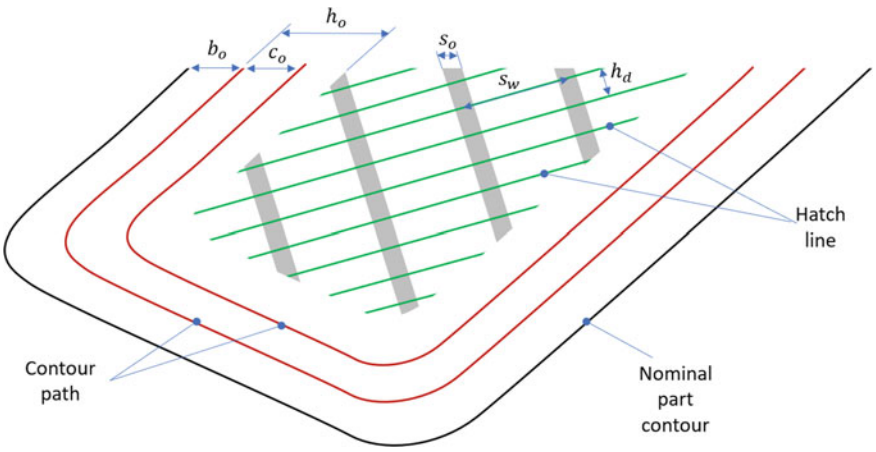

Fig. 1 Part layer, contour path, hatch lines schematization

the nominal part contour. Generally, more than one contours are generated moving furtherly the path. This parameter is called contour offset h_o. The filling of the part is provided by the hatching which moves the laser beam along parallel paths, namely the hatch lines, with properly defined energy. The interface between contours and hatching area is tailored by setting the hatch offset which defines the limit of the enclosed area. The hatch lines are organized in an exposure pattern. In the case of AlSi10Mg the hatching is exposed in stripes. In order to reduce the in-layer residual stress, a maximum hatch line length, namely the stripe width s_w, is set. The obtained discontinuity is reduced by an overlapping between lines called s_o. The distance between the lines is called hatch distance h_d.

This parameter, together the laser power P and the layer thickness L, is involved in the well-known formula of Volumetric Energy Density (VED):

$$VED = \frac{P}{Lvh_d} \tag{1}$$

where v is the scan speed. For the contour Eq. (1) cannot be applied thus the Linear Energy Density (LED) is used:

$$LED = \frac{P}{v} \tag{2}$$

The hatching of the top and the bottom of the part is no longer inside the part itself thus requiring different exposure settings. For the purpose the infill is divided into three categories: the upskin (zone over which no area to be exposed is present), the infill (interior area) and the downskin (zone under which no area to be exposed is present). The upskin and downskin thickness is defined by the number of layers

assigned to these categories. An overlap between infill and upskin/downskin is assigned to cover the discontinuity. In Fig. 2 a representation of these zones is shown.

In this work a laser remelting of the part skin was performed. The consolidation of the specimen was obtained using EOS standard process parameters for AlSi10Mg. The used layer thickness was 30 μm and hatching and contour had the processing parameters set reported in Table 2. As shown the infill, the upskin and the downskin are processed at about the same VED, i.e. 50, 57 and 47 J/mm^3 respectively pair to a LED of about 0.3 J/mm. Conversely the contour, which is composed by two similar scans, is characterized by a very small energy: the LED is reduced to 0.09 J/mm.

Aim of this work is to investigate how to improve the surface roughness of the part by providing a skin laser remelting. A typical approach to consider factors' level is the VED and LED for upskin and contour respectively. In [12] a fractional experimental plan was done varying scan speed between 800 and 1250 mm/s, setting the hatch distance at 0.15 and 0.20 mm and the power in the range 120–190 W (limited by the maximum system value); the resulting VED was in the range 24–79 J/mm^3. In [13] authors employed a greater laser power and investigated process outcome accordingly to manufacturer's standard parameters: the correspondent VEDs were: 50, 57, 133 J/mm^3. In the present work a wide range of VED for upskin is investigated: varying processing parameters at the three levels reported in Table 3, the VED ranges between 28 and 167 J/mm^3. Figure 3a shows the slice contour plot of VED: it is well evident that the considered factors levels allow having distinct energy

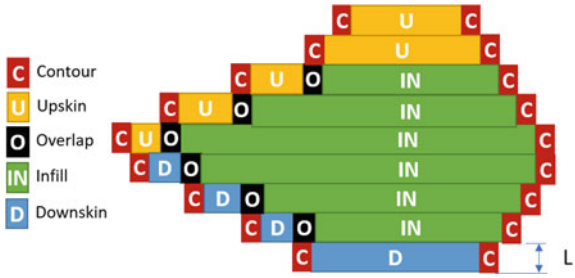

Fig. 2 Part vertical section: contour (C), upskin (U), overlap (O), downskin (D) and infill (IN) zones

Table 2 Process parameters for the consolidation of the part

Hatch				Contour	
Infill		Upskin		1	
P (W)	370	P (W)	360	P (W)	80
V (mm/s)	1300	V (mm/s)	1000	V (mm/s)	900
Hd (mm)	0.19	Hd (mm)	0.21	Co (mm)	0.02
Ho (mm)	0.02	Downskin		2	
Sv (mm)	0.02	P (W)	340	P (W)	85
Sw (mm)	7	V (mm/s)	1150	V (mm/s)	900
So (mm)	0.02	Hd (mm)	0.21	Co (mm)	0

Table 3 Experimented process parameters for upskin and contour strategy

Upskin				Contour			
Factors	Levels			Levels			
P (W)	240	300	360	P (W)	150	250	350
V (mm/s)	400	800	1200	V (mm/s)	400	800	1200
Hd (mm)	0.18	0.21	0.24	Co (mm)	0	0.02	0.04

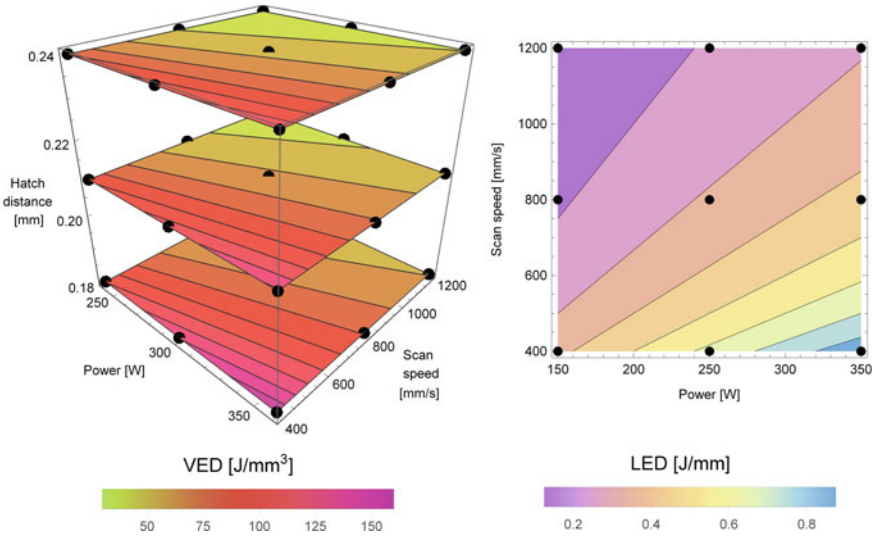

Fig. 3 VED (**a**) and LED (**b**) as a function of process parameters

values. As regards the contour, the work [14] reports several experimentations on vertical surfaces suggesting a LED in the range 0.46–0.74 J/mm: at higher energy, i.e. 0.82 J/mm, the Marangoni convection is enough strong to disturb the molten pool and fluctuations appear. Thus, in the present experimentation the range 0.125–0.875 J/mm was chosen. The relative process parameters are reported in Table 3 and represented in Fig. 3b.

The designed specimen and the fabricated ones are reported in Fig. 4. The geometry is characterized by horizontal, vertical and two inclined surfaces, 45 and 135°. The support structures were avoided on 135° overhanging surface and solid strategy was applied to the underside of the specimen.

The building platform was kept at 160 °C during the fabrication process in order to reduce residual stresses and no laser conditioning was applied to infill areas thus maintaining bulk properties of the fabricated specimen. For the purpose also the between-layer hatch strategy, such as the hatch rotation of 67°, was left unchanged. The specimens were oriented by 5° and fuzzy placed onto the platform so that the recoater concurrent hits were reduced; the exposure order was set against the argon

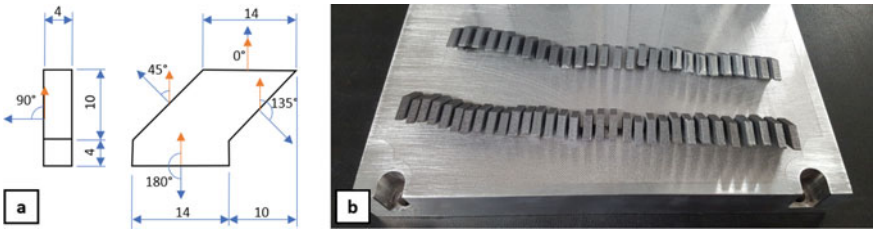

Fig. 4 Designed specimen (**a**) and fabricated specimens (**b**)

flow to avoid processing smoke onto powder surfaces going to be scanned. A replication of each parameter set combination was provided so that a total of 54 specimens were built. In addition, some specimens were fabricated without remelting for comparison. After the fabrication a thermal treatment for 2 h at 300 °C was performed in order to reduce deformation during the detachment from the building platform. This cutting operation was provided by an abrasive metallographic cutting machine: a SiC abrasive wheel 400 mm in diameter was used at 40 m/s cutting speed and 20 mm/min feed speed. No finishing operation, such as shot peening, was applied in order to leave the original SLMed surfaces.

2.3 Surface Measurements and Morphological Analysis

The roughness measurements were performed by a Mitutoyo Surftest SJ-412: the sampling length and the evaluation length were set at 2.5 and 12.5 mm, respectively [20]. A 2-μm stylus, sampling every 1.5 μm, was employed. The data were processed by a spline profile filter [21] with a cut-off λ_c and a short wavelength cut-off λ_s equal to 2.5 mm and 8 μm, respectively. The roughness profile parameters were calculated according to [22].

The morphological analysis was provided through an optical microscope. Each specimen was sectioned by a Struers Labotom-5 abrasive cutting equipment and polished by a Struers Labopol-2. The sections and the surfaces were captured by a Dino-Lite digital microscope with a polarized filter to remove the unwanted reflection or glare from the shiny object surface. An extension of the depth of field was obtained by moving the object along the optical axis and restored by wavelet-based image fusion technique [23].

3 Results

3.1 Upskin

The upskin strategy affects the surface quality of horizontal surfaces. According to the prediction model reported in [10], the attainable average roughness is about 7 μm. The specimen without remelting, i.e. a specimen fabricated with the standard processing parameters, was analyzed by means of roughness measurements (Fig. 5a). The average roughness is 7.57 μm very close to the expected value, and the total roughness R_t is more than 8 times this value highlighting the presence of local high peaks. In fact, the amplitude density function of the profile heights is characterized by pronounced tails; moreover, around the mean line a large spread is observed. This distribution is symmetrical (R_{sk} about zero) and the peakedness is leptokurtic (R_{ku} equal to 3.43). The mean spacing is 0.26 mm. This profile is characterized by a low reflectiveness as quantified by the Δ_q pair to 0.29, i.e. about 16°.

As a remelting is applied with a high VED (Fig. 5b) the roughness is improved: the defects are reduced as confirmed by an R_a pair to 2.8 μm and a R_t less than 6 times greater; the reflectiveness is improved to a Δ_q pair to 0.05 that is about 3°. The height distribution is now slightly platykurtic, the mean spacing is 0.57 mm. At 1200 mm/s scan speed (Fig. 5c) some local peaks are observed leading to an intermediate result for the average roughness and the reflectiveness. By increasing the VED at 139 J/mm^3 (with the process parameters set reported in Fig. 5d) a 76% decreasing in R_a with respect to the as is specimen is obtained. As expected, if the

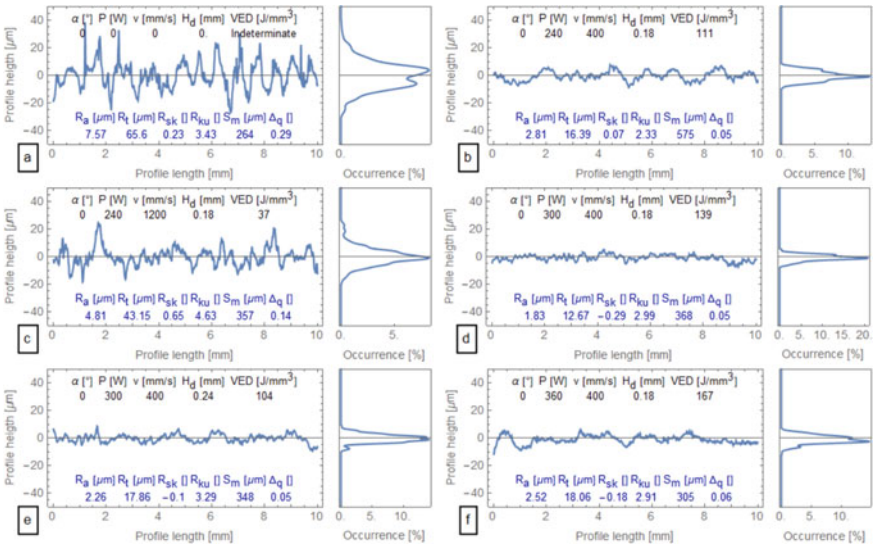

Fig. 5 Roughness profiles and amplitude density functions for different upskin remelting conditions

hatch distance is increased (VED pair to 104 J/mm^3), a reduced improvement is provided (Fig. 5e). As the VED is increased by a power of 360 W (Fig. 5f) the R_a is 2.52 μm suggesting that the decreasing in R_a is not linearly dependent upon the VED. The main effect plot can help in this investigation (Fig. 6a). As expected, the increasing of the power can lead to a decreasing of the R_a even if the effects at 300 and 360 W are the same; a marked increase is obtained by increasing the speed; conversely the hatch distance is slightly affecting the R_a. Both the VED and LED show a relationship with the R_a. In particular a local minimum is obtained at about 140 J/mm^3. In Fig. 6b, the box plot for different processing parameters values is displayed. It can be assessed that the best condition is found at 300 W power, 400 mm/s scan speed and 0.18 mm hatch distance but also applying 360 W at 400 and 800 mm/s a relevant improving is achieved.

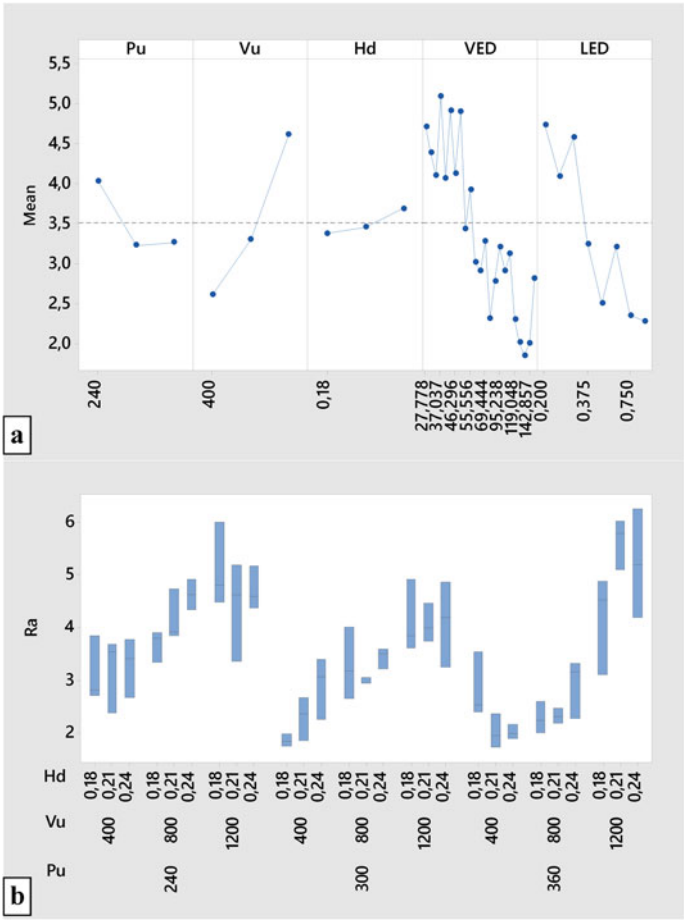

Fig. 6 Main effect plot (**a**) and box plot (**b**) for the experimented upskin process parameters

In the metallographic analysis the presence of defects will address the choice far from the highest VED levels. The analysis of variance (ANOVA) reported in Table 4 highlights that the hatch distance is not significant while the power, the scan speed and their interaction significantly affect the R_a (p-value < 0.01).

Fabricated surfaces were analyzed by means of morphological behavior. In Fig. 7a the specimen not subjected to remelting is shown. As expected, the presence of balling and satellite is observed. As a little specific energy is applied these defects decrease in dimension and occurrence (Fig. 7b). The laser tracks are herewith well evident but instable causing big pores: this is probably due to the strong Marangoni convection. At about 60 J/mm^3 the roughness improvement is accompanied by sparse balling (Fig. 7b) and unexpected thermal cracks at large hatch spacing (Fig. 7c). The number

Table 4 ANOVA table for the upskin data

Source	DF	SS	MS	F	P
Pu	2	11.079	5.5395	17.08	0.000
Vu	2	55.760	27.8801	85.94	0.000
Hd	2	1.407	0.7037	2.17	0.124
Pu * Vu	4	9.934	2.4836	7.66	0.000
Pu * Hd	4	0.305	0.0762	0.23	0.918
Vu * Hd	4	0.896	0.2239	0.69	0.602
Pu * Vu * Hd	8	6.955	0.8694	2.68	0.015
Error	54	17.517	0.3244		
Total	80	103.854			
S = 0.569557, R^2 = 83.13%, adj R^2 = 75.01%					

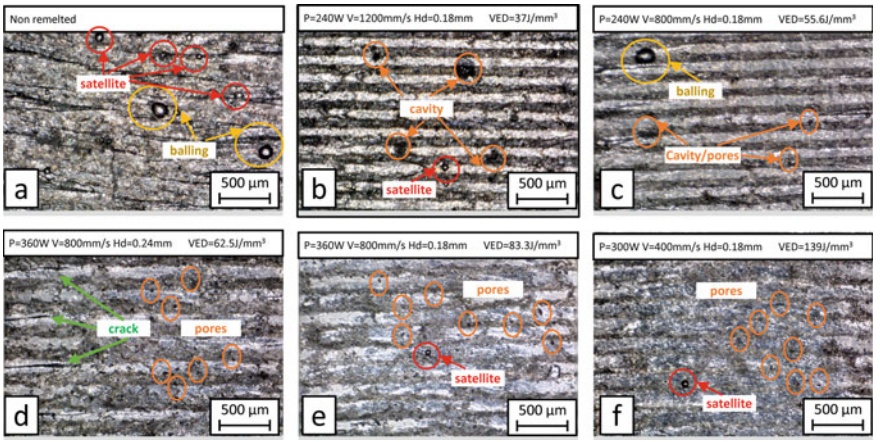

Fig. 7 Morphologies of horizontal surfaces without remelting (**a**) and at different remelting conditions (**b**–**f**)

of pores, probably due to shrinkage, increases. The adhering particles are reduced and laser tracks are smooth. Thermal cracks and almost all the defects disappear as the VED increases to 83 J/mm^3 (Fig. 7d) and 139 J/mm^3.

3.2 Contours

The vertical and the inclined surfaces are typically characterized by a very rough surface. According to the model [10], the vertical one is characterized by 22 μm R_a: this is confirmed by the profile reported in Fig. 8a: the distribution is symmetrical and Gaussian (R_{sk} about 0 and R_{ku} about 3) indicating a chaotic behavior of the profile heights. If a small LED is applied (Fig. 8b) the surface is slightly affected by the conditioning: the R_a is about unchanged, the distribution is leptokurtic and asymmetric since it moves downwards indicating an emptied profile. Negligible changing is observed if contour offset is modified. If the LED is increased by increasing power, the profile slightly worsens as reported in Fig. 8c. At this particular linear energy, if the contour offset is set to zero, an impressive changing is observed: the R_a is 4.2 μm and the peak to valley height is more than one quarter of millimeter (Fig. 8d). When the LED is more than 0.4 J/mm a marked improving in surface roughness is obtained. The process conditions reported in Fig. 8e provide an R_a under 5 μm and no variation is observed at different contour offset. At higher LED levels negligible differences are experienced as shown in Fig. 8f. The ANOVA analysis (Table 5) confirms this

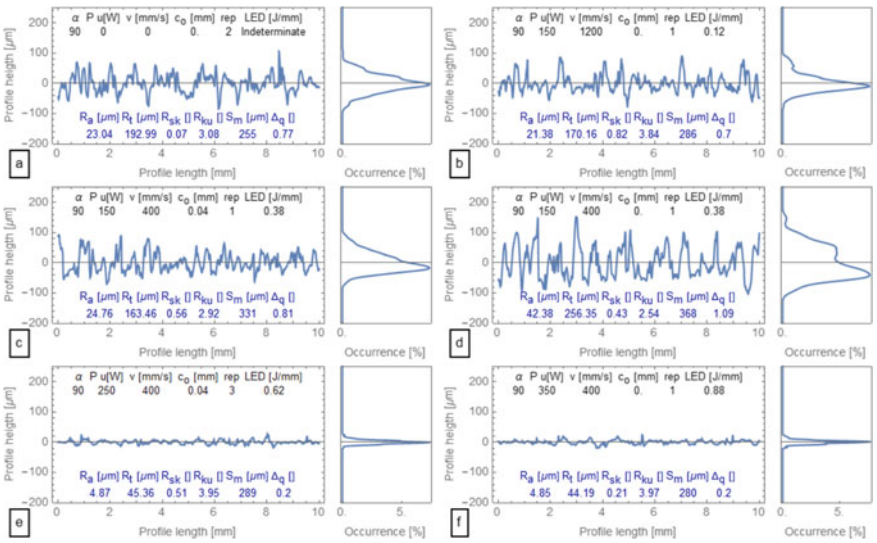

Fig. 8 Roughness profiles and amplitude density functions for different contour remelting conditions

Table 5 ANOVA table for the contour data

Source	DF	SS	MS	F	P
Pc	2	2616.47	1308.24	168.95	0.000
Vc	2	698.70	349.35	45.12	0.000
Co	2	70.06	35.03	4.52	0.015
Pc * Vc	4	2540.54	635.14	82.03	0.000
Pc * Co	4	364.95	91.24	11.78	0.000
Vc * Co	4	106.61	26.65	3.44	0.014
Pc * Vc * Co	8	70.92	8.86	1.14	0.349
Error	54	418.13	7.74		
Total	80	6886.39			
$S = 2.7826$, $R^2 = 93.93\%$, adj $R^2 = 91.00\%$					

intricate behavior assessing that the R_a is significantly affected by the factors and most of their interactions.

From the main effect plots (Fig. 9a) the expected trends for processing parameters are observed. The LED confirms a wave trends with a marked decreasing at high values. The box plots (Fig. 9b) suggest three scenarios corresponding to more than 70% roughness reduction: at {350 W, 400 mm/s, 0.04 mm}, at {250 W, 800 mm/s, 0.04 mm}, at {350 W, 800 mm/s, 0 mm}.

The untreated vertical surfaces are characterized by a generalized presence of balling as evidenced in Fig. 10a. The Marangoni convection here is so strong that the application of a mild linear energy, i.e. 0.125 J/mm, does not take effect (Fig. 10b). If a LED of 0.375 J/mm is applied the energy causes instabilities and generates local structures of balling coming from different layers (Fig. 10c). When the linear energy exceeds a threshold, the stability is no longer influenced by the LED and surface quality is markedly increased. Figure 10d shows the outcome at maximum power, intermediate scanning speed and contour offset pair to zero, which corresponds to a LED of 0.625 J/mm.

The same analysis can be carried out for surfaces inclined by 45 and 135°. The former is characterized by a 23 μm R_a in the non-treated case. This slope is markedly affected by the upper side of the contour and in most of the considered parameters set the remelting is not effective like in the vertical and horizontal surfaces. As evidenced in the main effect plot of Fig. 11a, the behavior with main processing parameters is not expected and ANOVA assesses the power and the speed are not significantly affecting the outcome. As regards the LED, two scenarios can be suggested: {250 W, 400 mm/s, 0 mm} and {350 W, 800 mm/s, 0 mm}. In these conditions the R_a is reduced to 16.5 μm.

In the case of 135° the starting R_a is 47 μm. Also in this case the ANOVA highlights an heterogeneous behaviour (Fig. 11b) and the LED can be used to find a minimum: the suggested scenario is: {250 W, 800 mm/s, 0 mm} with a reduction of 24%.

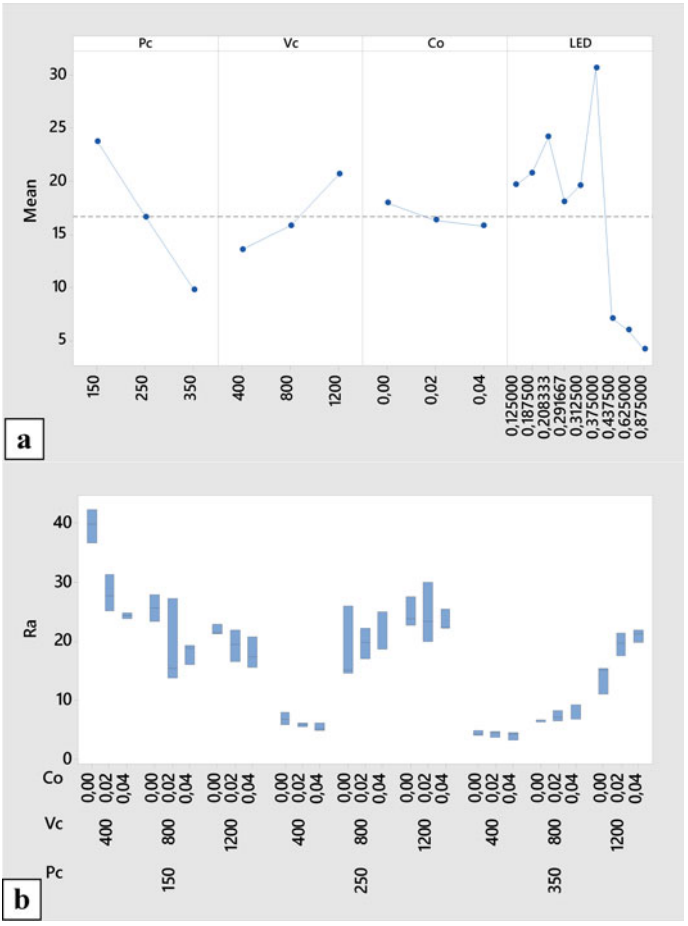

Fig. 9 Main effect plot for vertical surfaces (**a**) and box plot (**b**) for the experimented contour process parameters

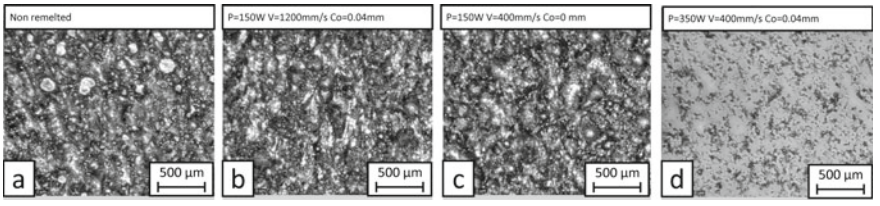

Fig. 10 Morphologies of vertical surfaces without remelting (**a**) and at different remelting conditions (**b–d**)

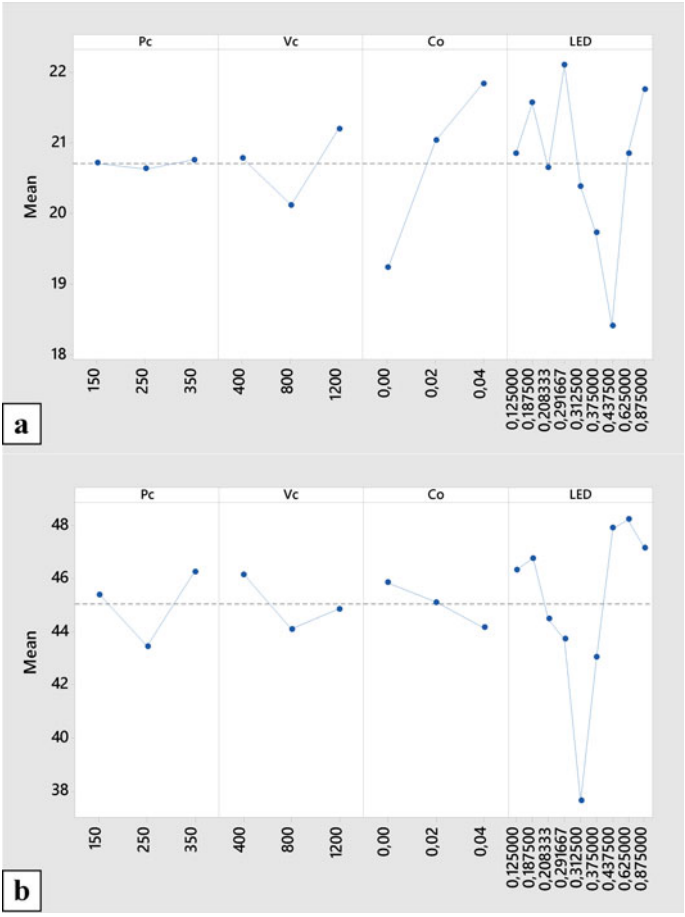

Fig. 11 Main effect plots of the experimented contour process parameters for surfaces characterized by 45° (**a**) and 135° (**b**)

The morphological analysis confirms the marginal improvement of selected processing parameters. In Fig. 12a the not remelted surface is fully characterized by balling phenomena. At a LED pair to 0.62 J/mm a scattering of defects is observed (Fig. 12b). For overnaging surfaces the peaks are twice the previous case and cannot be detected on Fig. 12c. This surface needs less specific energy, i.e. 0.31 J/mm, to find a good combination of processing parameters which may reduce the balling phenomena.

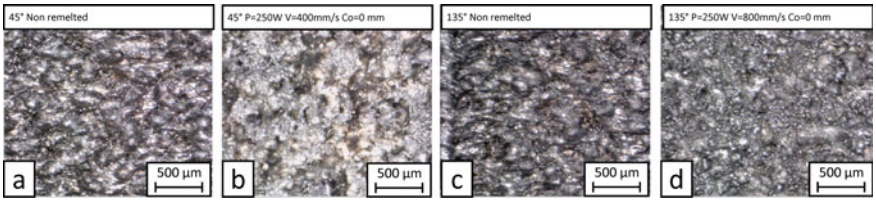

Fig. 12 Morphologies of inclined surfaces without remelting (**a**, **c**) and with remelting (**b**, **d**)

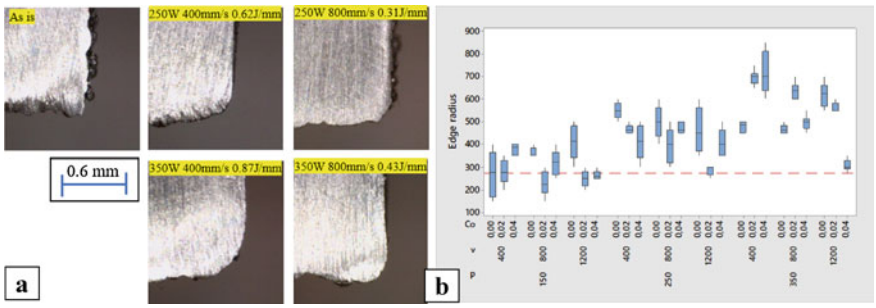

Fig. 13 Fabricated edges for different experimented conditions (**a**); box plot of edge radii (µm) (**b**)

3.3 Edge Deviation

The remelting leads to a modification of micro-geometry which may affect also the shape of the specimen. This is well evident if the edges are considered. A not treated specimen shows a mean edge radius of 0.275 mm (Fig. 13a). This deviation is typical of aluminum alloys which present the issues claimed in the introduction. When the LED is low this deviation is almost maintained (less than 0.5 J/mm). If the remelting is carried at 0.87 J/mm (350 W and 400 mm/s) a big radiusing occurs: in this condition 0.7–0.8 mm is measured and it must be checked if it is tolerated by the part design. The LED is not a reliable way to understand this behavior: an exception occurs at middle value (350 W, 1200 mm/s, 0.04 mm) where the measured radius ranges between 0.6 mm and 0.7 mm. The undertaken measures are reported in the box plot of Fig. 13b. It is well evident that the power must be kept at 250 W and some of the previous scenarios are preferred.

4 Conclusions

In this paper the effects of a skin laser remelting of AlSi10Mg parts fabricated by SLM was studied. Different process parameters for different scan strategies were

experimented in order to improve the obtainable surface roughness for horizontal, vertical and inclined surfaces. The upskin strategy influenced the quality of the horizontal ones. The best result for the roughness was obtained for the parameters set 300 W power, 400 mm/s scan speed and 0.18 mm hatch spacing with a reduction more than 75% with respect to the as is specimen. The contour strategy influenced the surface quality of both vertical and inclined surfaces. For these surfaces, different behaviors at different experimented process parameters were observed. The best surface quality for the vertical surfaces were attained at higher LED values. The suggested parameters set were {350 W, 400 mm/s, 0.04 mm}, {250 W, 800 mm/s, 0.04 mm}, at {350 W, 800 mm/s, 0 mm} corresponding to a roughness reduction of more than 70%. Conversely for the two inclined surfaces the remelting was not so effective. For 45°, two scenarios were suggested {250 W, 400 mm/s, 0 mm} and {350 W, 800 mm/s, 0 mm} that correspond to a reduction about 28%; for 135° the minimum roughness was found for the parameters set {250 W, 800 mm/s, 0 mm} with a reduction of 24% than the as is case. The shape was analyzed highlighting that high energy values determine defects on the edges shape. To reduce these effects a power reduction must be considered helping the choice of suitable scenarios of the contour strategy for both vertical and inclined surfaces.

The effectiveness of the proposed remelting methodology is accompanied by a small increase of building time: the simulation over the well-known NIST benchmark artefact [24] required only 2% additional building time with respect to the fabrication without remelting.

Further investigations will regard the application of different process parameters set to all the possible inclinations.

References

1. ISO/ASTM52900-15 (2015) Standard terminology for additive manufacturing—general principles—terminology. ASTM International, West Conshohocken
2. Gu D (2015) Laser additive manufacturing of high-performance materials. Springer-Verlag, Berlin Heidelberg
3. Martin JH, Yahata BD, Hundley JM, Mayer JA, Schaedler TA, Pollock TM (2017) 3D printing of high-strength aluminium alloys. Nature 549:365–369
4. Jung JG, Lee SH, Cho YH, Yoon WH, Ahn TY, Ahn YS, Lee JM (2017) Effect of transition elements on the microstructure and tensile properties of Al–12Si alloy cast under ultrasonic melt treatment. J Alloys Compd 712:277–287
5. Jung JG, Ahn TY, Cho YH, Kim SH, Lee JM (2018) Synergistic effect of ultrasonic melt treatment and fast cooling on the refinement of primary Si in a hypereutectic Al–Si alloy. Acta Mater 144:31–40
6. Louvis E, Fox P, Sutcliffe CJ (2011) Selective laser melting of aluminium components. J Mater Process Technol 211:275–284
7. Gusarov AV, Kruth JP (2005) Modelling of radiation transfer in metallic powders at laser treatment. Int J Heat Mass Transfer 48(16):3423–3434
8. Fischer P, Karapatis N, Romano V, Glardon R, Weber HP (2002) A model for the interaction of near-infrared laser pulses with metal powders in selective laser sintering. Appl Phys A Mater 74(4):467–474

9. Zhang J, Song B, Wei Q, Bourell D, Shi Y (2019) A review of selective laser melting of aluminum alloys: processing, microstructure, property and developing trends. J Mater Sci Technol 35(2):270–284
10. Boschetto A, Bottini L, Veniali F (2017) Roughness modeling of AlSi10Mg parts fabricated by selective laser melting. J Mater Process Technol 241:154–163
11. Xiang Z, Wang L, Yang C, Yin M, Yin G (2019) Analysis of the quality of slope surface in selective laser melting process by simulation and experiments. Optik 176:68–77
12. Calignano F, Manfredi D, Ambrosio EP, Iuliano L, Fino P (2013) Influence of process parameters on surface roughness of aluminum parts produced by DMLS. Int J Adv Manuf Technol 67:2743–2751
13. Mohammadi M, Asgari H (2018) Achieving low surface roughness AlSi10Mg_200C parts using direct metal laser sintering. Addit Manuf 20:23–32
14. Yang T, Liu T, Liao W, MacDonald E, Wei H, Chen X, Jiang L (2019) The influence of process parameters on vertical surface roughness of the AlSi10Mg parts fabricated by selective laser melting. J Mater Process Technol 266:26–36
15. Boschetto A, Bottini L, Veniali F (2018) Surface roughness and radiusing of Ti6Al4V selective laser melting-manufactured parts conditioned by barrel finishing. Int J Adv Manuf Technol 94:2773
16. Yasa E, Kruth J (2011) Application of laser re-melting on selective laser melting parts. Adv Prod Eng Manag 6:259–270
17. Liu B, Li BQ, Li Z (2019) Selective laser remelting of an additive layer manufacturing process on AlSi10Mg. Results Phys 12:982–988
18. Demir AG, Previtali B (2017) Investigation of remelting and preheating in SLM of 18Ni300 maraging steel as corrective and preventive measures for porosity reduction. Int J Adv Manuf Technol 93:2697–2709
19. Vaithilingam J, Goodridge RD, Hague RJM, Christie SDR, Edmondson S (2016) The effect of laser remelting on the surface chemistry of Ti6Al4V components fabricated by selective laser melting. J Mater Process Technol 232:1–8
20. ISO 4288-08 (E) (1996) Geometrical product specifications (GPS)—surface texture: profile method—rules and procedures for the assessment of surface texture. International Organization for Standardization (ISO), Geneva
21. ISO 16610-22 (2015) Geometrical product specifications (GPS)—filtration—part 22: linear profile filters: spline filters. International Organization for Standardization (ISO), Geneva
22. ISO 4287 (1997) Geometrical product specification (GPS)—surface texture: profile method—terms, definition and surface texture parameters. International Organization for Standardization (ISO), Geneva
23. Forster B, Van De Ville D, Berent J, Sage D, Unser M (2004) Complex wavelets for extended depth-of-field: a new method for the fusion of multichannel microscopy images. Microsc Res Technol 65:33–42
24. Moylan, SP, Slotwinski JA, Cooke AL, Jurrens KK, Donmez MA (2012) Proposal for a standardized test artifact for additive manufacturing machines and processes. In: Proceedings of the 23rd international solid free form symposium—an additive manufacturing conference, Austin, Aug 2012, pp 902–920